NJC

Accepted Manuscript

This is an *Accepted Manuscript*, which has been through the Royal Society of Chemistry peer review process and has been accepted for publication.

Accepted Manuscripts are published online shortly after acceptance, before technical editing, formatting and proof reading. Using this free service, authors can make their results available to the community, in citable form, before we publish the edited article. We will replace this *Accepted Manuscript* with the edited and formatted *Advance Article* as soon as it is available.

You can find more information about *Accepted Manuscripts* in the Information for Authors.

Please note that technical editing may introduce minor changes to the text and/or graphics, which may alter content. The journal's standard Terms & Conditions and the Ethical guidelines still apply. In no event shall the Royal Society of Chemistry be held responsible for any errors or omissions in this *Accepted Manuscript* or any consequences arising from the use of any information it contains.

ROYAL SOCIETY OF CHEMISTRY

www.rsc.org/njc

New Journal of Chemistry

Dynamic Article Links ►

Cite this: DOI: 10.1039/c0xx00000x

www.rsc.org/xxxxxx

Paper

Proteasome inhibition and cytostatic effects to human cancer cells by pyrazolone-enamines: a combined crystallographic, structural and computational study†

Xingchen Yan,[a,b] Jiakun Xu,[c,a] Xiaojing Wu,[a] Zhongyu Zhang,[a] Xia Zhang,[a] Yuhua Fan*[a] and Caifeng Bi*[a]

Received (in XXX, XXX) Xth XXXXXXXXX 20XX, Accepted Xth XXXXXXXXX 20XX
DOI: 10.1039/b000000x

Nine compounds were designed and synthesized by the condensation reaction of the carbonyl in 4-benzoyl-3-methyl-1-phenyl-2-pyrazolin-5-one (HPMBP) with the amino groups in 5-aminoisophthalic acid, 4,4′-diaminodiphenylmethane, 4-aminophenylacetic acid, 4-aminobenzamide, 2-amino-4-methylphenol, 5-amino-2-methylphenol, 2-aminophenol, 3-aminophenol and 4-aminophenol respectively. They were then characterized by IR, ^{1}H NMR, elemental analysis, and X-ray crystallography, which suggest that all of them exist as the pyrazolone-enamine forms in the solid state and DMSO solution through tautomeric reactions. The nine compounds (compounds **1** ~ **9**) were evaluated for their ability to inhibit the proliferation of human liver cancer HepG2 cells. Compounds **5**, **6, 7** and **8** demonstrate strong inhibitory effect to the proliferation of HepG2 cells. The nine compounds can also inhibit the activity of human cancer cellular 20S proteasome. Further studies on compound **6** as the representative indicate that it can cause the accumulation of ubiquitinated proteins and the proteasome target proteins Bax and p27, and exhibit cytostatic effect to HepG2 cells in a concentration-dependent and time-dependent manner. The four potential tautomers of compound **6** were optimized and their single point energies were calculated by Density Functional Theory (DFT) B3LYP method based on the Polarized Continuum Model (PCM) in water to identify the most likely existed tautomer in cancer cells. Based on the optimized structure of the most stable tautomer in water, the Wiberg bond orders, molecular electrostatic potential (MEP) maps and frontier molecular orbital were calculated. As compounds **5**, **6, 7** and **8** have hydroxyl in the *ortho*-position or *meta*-position, our study can provide some information to study their anticancer mechanism and the substitution effect of different functional groups.

Introduction

Pyrazolines derivatives have attracted intensive attentions during the past decades for their potentials as antibacterial,[1] antifungal,[2] cyclooxygenase (COX-2),[3] anti-inflammatory,[4] antidiabetic,[5] anticonvulsant,[6] antitumoral[7] and antiHIV[8] agents. Within this class, 4-acyl-5-pyrazolones are extensively studied as analgesics, anti-inflammatory agents, antipyretics and insecticides.[9] 4-Benzoyl-3-methyl-1-phenyl-2-pyrazolin-5-one (HPMBP) and its derivatives are pervasively used for trace metal separating,[10–13] sterilizing and deinsectizing.[14] As a *β*-diketone, HPMBP may exist as four tautomers as shown in Scheme 1.[15]

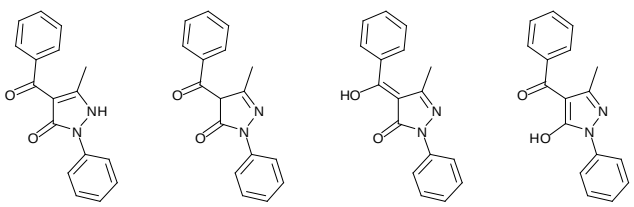

Scheme 1 Four tautomers of HPMBP.

Schiff bases (azomethines) represent one of the most widely used classes of organic compounds. Due to the presence of imine (–N=CH–) group which is similar to the structures in natural biological system, they play a key role in studying the mechanism of transformation and rasemination reaction in biological systems.[16–24] Schiff bases are reported to show many important biological activities such as antibacterial,[25] anti HIV,[26] antifungal,[27] antiviral,[28] antimosquito larvae,[29] antiflamatory,[30] antitumor[31] and anticancer[32] activities. As a result, we surmised that the Schiff bases derived from HPMBP should have bioactivities. We then selected HPMBP to react with 5-aminoisophthalic acid, 4,4′-diaminodiphenylmethane, 4-aminophenylacetic acid, 4-aminobenzamide, 2-amino-4-methylphenol and 5-amino-2-methylphenol, respectively, and obtained six new single crystals from the ethanol or methanol solution. Characterized by IR, ^{1}H NMR, elemental analysis, and X-ray crystallography, the six compounds, 4-[(*Z*)-(3,5-dicarboxyphenylamino)phenylmethylene]-3-methyl-1-phenyl-2-pyrazolin-5-one (**1**), 4-{(*Z*)-[4-(4-aminobenzyl)phenylamino] phenylmethylene}-3-methyl-1-phenyl-2-pyrazolin-5-one (**2**), 4-

{(*Z*)-[4-(carboxymethyl)phenylamino]phenylmethylene}-3-methyl-1-phenyl-2-pyrazolin-5-one (**3**), 4-{(*Z*)-[4-(aminocarbonyl)phenylamino]phenylmethylene}-3-methyl-1-phenyl-2-pyrazolin-5-one (**4**), 4-[(*Z*)-(2-hydroxy-5-methylphenylamino)phenylmethylene]-3-methyl-1-phenyl-2-pyrazolin-5-one (**5**) and 4-[(*Z*)-(3-hydroxy-4-methylphenylamino)phenylmethylene]-3-methyl-1-phenyl-2-pyrazolin-5-one (**6**), and the previously reported three compounds 4-[(*Z*)-(2-hydroxyphenylamino)phenylmethylene]-3-methyl-1-phenyl-2-pyrazolin-5-one (**7**), 4-[(*Z*)-(3-hydroxyphenylamino)phenylmethylene]-3-methyl-1-phenyl-2-pyrazolin-5-one (**8**) and 4-[(*Z*)-(4-hydroxyphenylamino)phenylmethylene]-3-methyl-1-phenyl-2-pyrazolin-5-one (**9**)[33] were found to exist as the pyrazolone-enamines formed by tautomeric reactions instead of Schiff bases in the solid state and DMSO solution (Scheme 2). However, compounds **5**, **6**, **7** and **8** still demonstrate strong inhibitory effect to the proliferation of human liver cancer HepG2 cells.

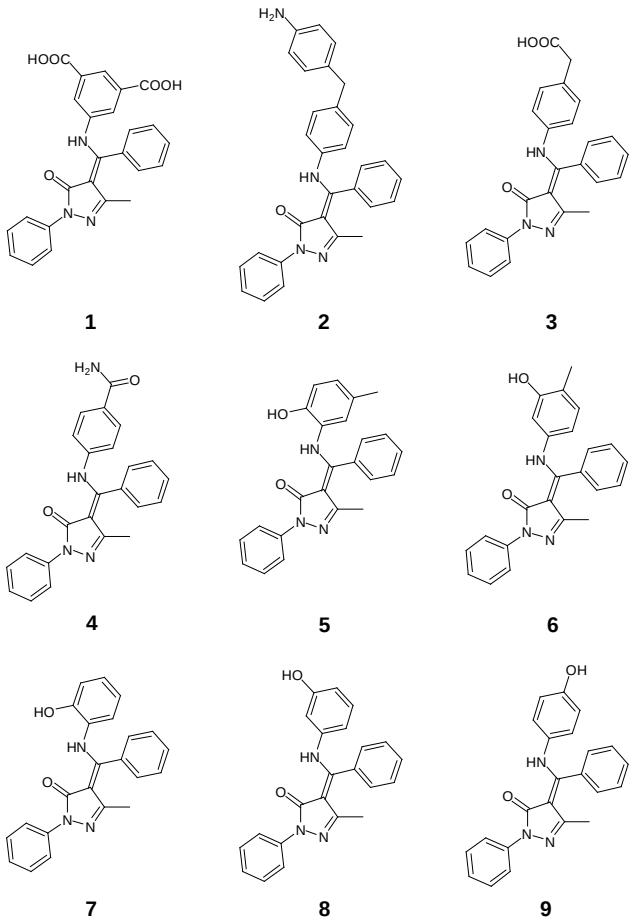

Scheme 2 Structures of compounds **1** ~ **9**.

The ubiquitin-proteasome system (UP-S) involves in a number of important cellular processes like cell proliferation and apoptosis, DNA damage and repair, drug resistance and differentiation, cycle progression and endocytosis.[34–36] Proteasome could be the target of novel anticancer drugs because it will have more impact on cancer cells than normal cells when its activity is inhibited.[37] The UP-S contains a protease complex with high molecular weight called 20S proteasome. The 20S proteasome has a proteolytic core containing β1, β2 and β5 subunits, which are respectively associated with three distinct catalytic activities: caspase-like, trypsin-like and chymotrypsin-like (CT-like) activities.[38,39] When the CT-like activity in tumor cells is inhibited through inhibition of the β5 proteasomal subunit, the apoptosis of tumor cells will be induced.[40–42] At the same time, an associated accumulation of target proteins will occur, followed by an induction of programmed cell death, or apoptosis.[43–45] Thus, the proteasome inhibitory ability of the nine compounds in human liver cancer HepG2 cells was investigated, and compound **6** was selected to carry on the further study.

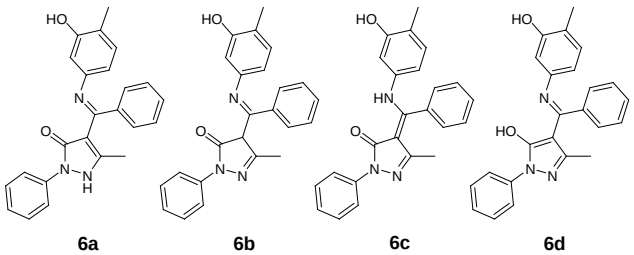

Scheme 3 Four tautomers of compound **6**.

Tautomerism in bioactive compounds plays a key role in orientation of bioactivity of drugs that have found wide application in drug design, from new medicinal materials to antibacterial imidazo[1,2-a]pyrimidine (-pyridine),[46] as sulphonamides in the antifungal agents[47] and as potential antiHIV spiroheterocycles.[48] Like HPMBP, compound **6** is also likely to exist as four tautomers (Scheme 3) in water, although it exists as tautomer **6c** in the solid state. To well understand the inhibitory mechanism and acting sites of compound **6** to 20S proteasome, raveling which tautomer that actually exists in the solution environment is indispensable. Thus, ^{1}H NMR spectra of the nine compounds were recorded to determine the position of the hydrogen. Then the four potential tautomers of compound **6** were optimized and their single point energies were calculated by Density Functional Theory (DFT) B3LYP method based on the Polarized Continuum Model (PCM) in water to identify the most likely existed tautomer in cancer cells. The substitution effect of different functional groups and possible inhibitory mechanism to the activity of 20S proteasome were discussed based on the experimental and computational results.

Results and Discussions

Description of crystal structures

The atomic labeling schemes for an asymmetric unit of compounds **1** ~ **6** are shown in Fig. 1. Comparison of the selected bond lengths of compounds **1** ~ **6** is listed in Table 1. Crystallographic data and structure refinement for compounds **1** ~ **6** are shown in Table S1 in the supplementary material. Selected bond lengths and angles for compounds **1** ~ **6** are listed in tables S2 ~ S7 in the supplementary material, respectively. Details of the hydrogen bonds for compounds **1** ~ **6** are listed in Tables S8 ~ S13 in the supplemenptary material, respectively. The crystal of compounds **1** ~ **4** have a supermolecular structure which is consisted of the molecules of the compounds and solvent molecules. In contrast, there exit no solvent molecules in the crystal lattice of compounds **5** and **6**. As a result, compounds **1**

and **6** are selected as the representatives to discuss.

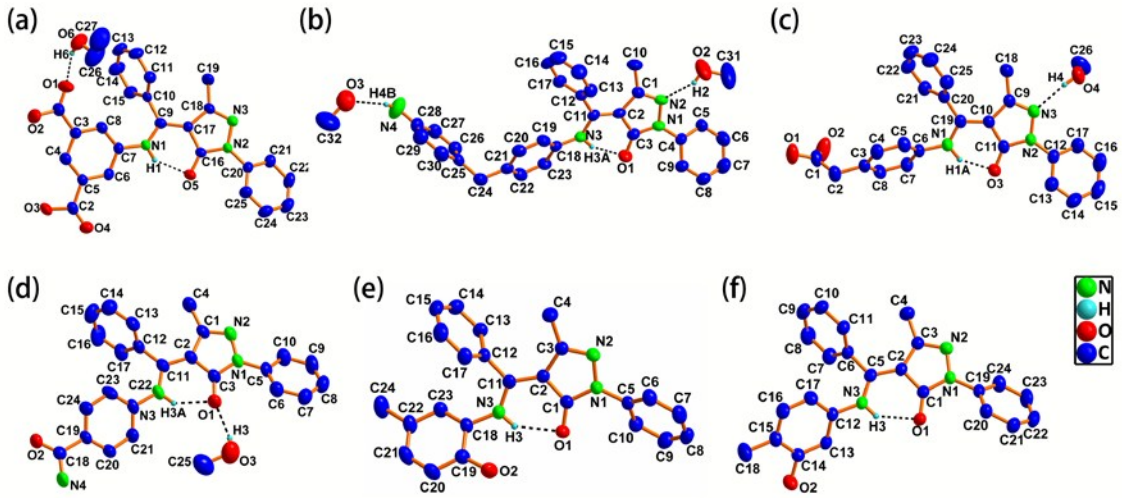

Fig. 1 The atomic labeling scheme for an asymmetric unit of (a) compound **1**; (b) compound **2**; (c) compound **3**; (d) compound **4**; (e) compound **5**; (f) compound **6**. All hydrogen atoms are omitted for clarity, except for those engaged in hydrogen bonding.

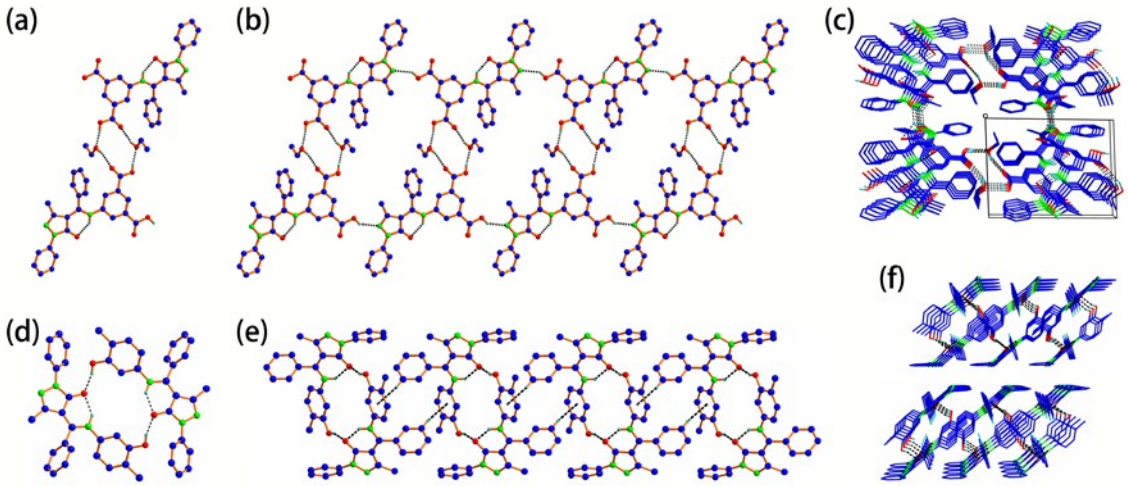

Fig. 2 (a) The tetramer connected by hydrogen bonding in compound **1**. (b) The 1-D chain structure of compound **1**. (c) The 3-D supermolecular structure of compound **1**. (d) The dimer connected by hydrogen bonding in compound **6**. (e) The 1-D chain structure of compound **6**. (f) The 3-D structure of compound **6**. All hydrogen atoms are omitted for clarity, except for those engaged in hydrogen bonding.

Table 1 Comparison of the selected bond lengths of compounds **1** ~ **6** (Å, °)

Bond	**1**	Bond	**2**	Bond	**3**	Bond	**4**	Bond	**5**	Bond	**6**
O5–C16	1.245(4)	O1–C3	1.249(5)	O3–C11	1.251(3)	O1–C3	1.253(4)	O1–C1	1.260(2)	O1–C1	1.261(2)
N3–C18	1.305(4)	N2–C1	1.308(6)	N3–C9	1.308(3)	N2–C1	1.309(5)	N2–C3	1.313(3)	N2–C3	1.308(2)
C9–C17	1.384(5)	C2–C11	1.377(7)	C10–C19	1.396(3)	C2–C11	1.410(5)	C2–C11	1.395(3)	C2–C5	1.400(2)
N2–C16	1.365(4)	N1–C3	1.361(6)	N2–C11	1.368(3)	N1–C3	1.383(5)	N1–C1	1.368(3)	N1–C1	1.367(2)
N2–N3	1.396(4)	N1–N2	1.395(5)	N2–N3	1.396(3)	N1–N2	1.406(4)	N1–N2	1.399(2)	N1–N2	1.400(2)
N1–C9	1.334(4)	N3–C11	1.344(6)	N1–C19	1.331(3)	N3–C11	1.340(5)	N4–C11	1.335(3)	N3–C5	1.329(2)
C16–C17	1.442(5)	C2–C3	1.436(6)	C10–C11	1.437(3)	C2–C3	1.439(5)	C1–C2	1.434(3)	C1–C2	1.436(2)
C17–C18	1.434(5)	C1–C2	1.431(6)	C9–C10	1.429(3)	C1–C2	1.445(5)	C2–C3	1.438(3)	C2–C3	1.439(3)

Compound **1** exists as the enamine formed through two steps (Fig. 1a). In the first step, the carbonyl in HPMBP condenses with the amino group in 5-aminoisophthalic acid to form the Shiff base (Scheme 4). Then the proton transfers from N3 to N1 through tautomeric reaction (Scheme 5) to form compound **1**. As shown in Table 1, The O5–C16, N3–C18, C9–C17, N1–C9, C16–C17, C17–C18 bond lengths indicate that O5–C16, N3–C18 and C9–C17 are double bonds while N1–C9, C16–C17 and C17–C18 are single bonds, which is consistent to the existence of H1 bonded to N1 (Fig. 1a). This suggests that the Schiff base structure obtained though the reaction of HPMBP with 5-aminoisophthalic acid has become the pyrazolone-enamine through tautomeric reaction. As a result, O5 and H1 are linked by intramolecular hydrogen bond N1–H1···O5 to form a hexatomic

ring O5–C16–C17–C9–N1–H1···O5, which make the O5–C16 and N1–H1 bonds coplanar. Meanwhile, two ethanol molecules and two carboxylic groups from two molecules of compound **1** are connected by the O–H···O hydrogen bonds to form a tetramer (Fig. 2a). Adjacent tetramers are connected through O–H···N hydrogen bonding to give rise to a 1-D chain structure (Fig. 2b). These chains are further connected through Van der Waals' force and π-π stacking interactions to form the 3-D supermolecular structure (Fig. 2c).

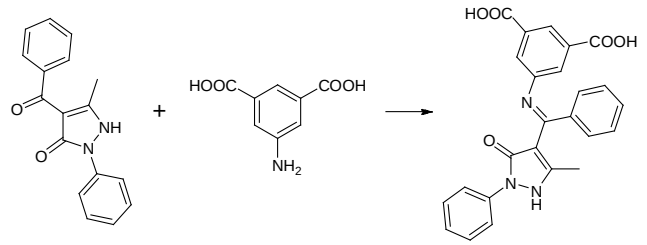

Scheme 4 Formation of the pyrazolone-imine form of compound **1**.

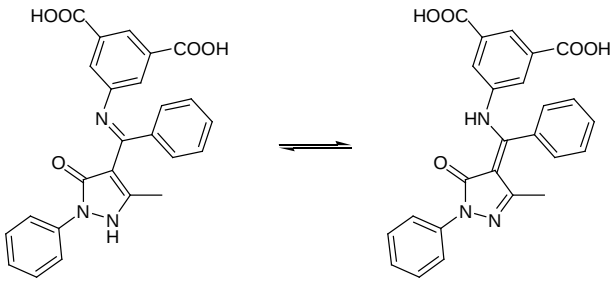

Scheme 5 the tautomeric reaction of compound **1**.

Compound **6** also exists as the enamine formed through the two-step reactions. As shown in Table 1, The O1–C1, N2–C3, C2–C5, N3–C5, C1–C2, C2–C3 bond lengths indicate that O1–C1, N2–C3 and C2–C5 are double bonds while N3–C5, C1–C2 and C2–C3 are single bonds, which is consistent to the existence of H3 bonded to N3 (Fig. 1f). As a result, O1 and H3 are linked through intramolecular hydrogen bond N3–H3···O1 to form a hexatomic ring O1–C1–C2–C5–N3–H3···O1, which makes the O1–C1 and N3–H3 bonds coplanar. Meanwhile, two molecules of compound **6** are connected by the O–H···O hydrogen bonding to form a dimer (Fig. 2d). Adjacent dimers are linked through C–H···π interactions to give rise to a 1-D chain structure (Fig. 2e). These chains are further connected through Van der Waals' force and π-π stacking interactions to form the 3-D structure (Fig. 2f).

Characterization of the position of the hydrogen atom is discussed in the supplementary material. The crystal structure and ^{1}H NMR spectra confirm the establishment of the pyrazolone-enamine forms of compounds **1** and **6** both in the solid state and in DMSO solution.

Anticancer studies

Viability assays of human liver cancer HepG2 cells

Human liver cancer HepG2 cells were treated with compounds **1** ~ **9** at different concentrations (25, 50 and 100 μM) for 24 h, followed by MTT assay. Cells treated with the solvent DMSO were used as control (Fig. 3). As MTT can be reduced to formazan by the nine compounds, the inhibitory effect measured by MTT assay is not accurate. However, repeated experiments all show that compounds **5**, **6**, **7** and **8** have better effect to inhibit the proliferation of HepG2 cells, and compound **6** exhibits the best effect to inhibit the proliferation of HepG2 cells ($p < 0.001$). As compounds **5**, **6**, **7** and **8** have hydroxyl in the *ortho*-position or *meta*-position, their anticancer activities should be related to these hydroxyl. However, compound **9** with hydroxyl in the *para*-position exhibits no anticancer activity. Fig. 4 shows the corresponding cellular morphological changes of human liver cancer HepG2 cells treated with compound **6** at different concentrations (25, 50 and 100 μM) for 24 h, and cells treated with the solvent DMSO were also used as control. When the concentration of compound **6** increased to 25 μM, almost all the cells are dead (shrunken and rounded up). When the concentration of compound **6** increased to 50 and 100 μM, part of the sample precipitated out (the black spot), so its concentration is also not accurate. As a result, we cannot obtain the quantitative results, but we can conclude that compound **6** exhibits the strongest inhibitory effect to the proliferation of human liver cancer HepG2 cells at the concentration of 25μM.

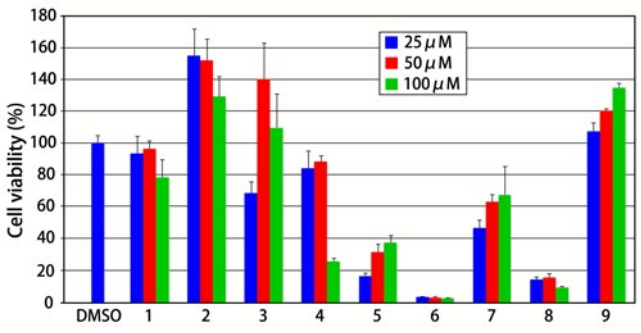

Fig. 3 Comparison of viability of human liver cancer HepG2 cells treated with the nine compounds, followed by MTT assay ($p < 0.001$).

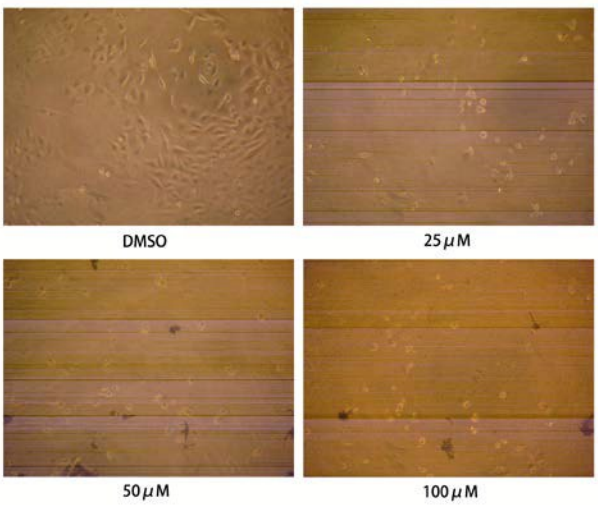

Fig. 4 Morphological changes of human liver cancer HepG2 cells treated with compound **6** at different concentrations (25, 50 and 100 μM) for 24 h (×100).

Inhibition to human cancer cellular 20S proteasomal CT-like activity in human liver cancer HepG2 cells

To investigate if the growth-inhibitory activity of the nine compounds are associated with their ability to inhibit the

proteasomal CT-like activity, human liver cancer HepG2 cells were treated with the nine compounds for 24 h at the concentration of 40μM (the maximum concentration that the nine compounds do not precipitate out) in the presence of fluorogenic substrate Suc-LLVY-AMC specific for the CT-like activity. Cells treated with the solvent DMSO were used as control (Fig. 5). The results show that all the nine compounds were able to inhibit the proteasomal CT-like activity in HepG2 cells ($p < 0.001$).

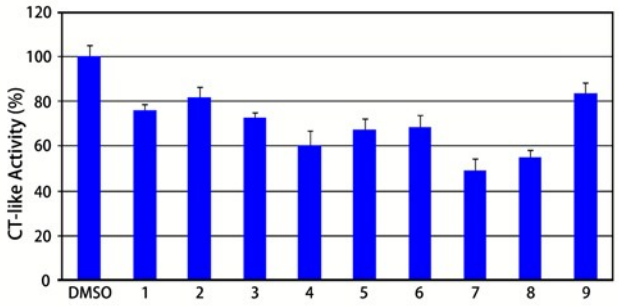

Fig. 5 The inhibition of CT-like activity in human liver cancer HepG2 cells treated with the nine compounds for 24 h at the concentration of 40 μM ($p < 0.001$).

Inhibition to the CT-like activity of purified 20S proteasome by compound 6

To make the quantitative study, purified rabbit 20S proteasome was treated with compound **6** in various concentrations (5, 10, 20 and 40 μM) for 24 h in the presence of fluorogenic substrate Suc-LLVY-AMC specific for the CT-like activity. Purified rabbit 20S proteasome treated with the solvent DMSO were used as control (Fig. 6a). The results indicate that compound **6** was capable of inhibiting proteasomal CT-like activity in a concentration-dependent manner, with the IC_{50} value of 9.8 μM ($p < 0.001$). Then we incubated compound **6** at the concentration of 40 μM for increasing time (0, 8, 16 and 24 h) in the presence of fluorogenic substrate Suc-LLVY-AMC specific for the CT-like activity (Fig. 6b). Compound **6** also inhibited the proteasomal CT-like activity in a time-dependent manner ($p < 0.001$). These data suggest that compound **6** could target the 20S proteasomal catalytic β5 subunit. L. da Costa Souza *et. al*. have reported the inhibitory effect of Black-eyed pea Trypsin/Chymotrypsin Inhibitor (BTCI) toward 20S proteasomal caspase-like, chymotrypsin-like and trypsin-like activities using MG132 as the positve control.[49] Both BTCI and MG132 demonstrate very effective inhibition to CT-like activities which decreases to about 15% at the concentration of 10 μM. In contrast, 50% CT-like activity is determined with the 10 μM concentration of compound **6**, which is worse than BTCI and MG132. There are also some transitional metal complexes as proteasome inhibitors. J. Zuo *et. al*. synthesized some amino acid Schiff base-copper complexes as the proteasome inhibitors.[34] Two of the complexes exhibit effective inhibition to purified 20S proteasomal CT-like activities with the IC_{50} values of 13.3 and 11.3 μM, respectively, In contrast, the IC_{50} value of compound **6** to inhibit proteasomal CT-like activity is 9.8 μM. However, many complexes have very high toxity to human body, and this is the shortcoming of complexes as proteasome inhibitors.

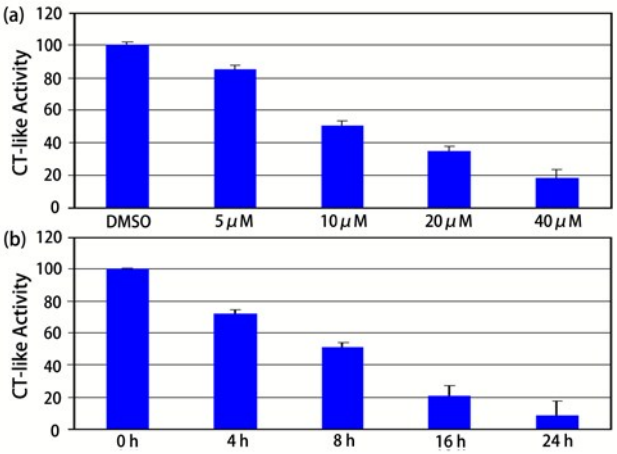

Fig. 6 The inhibition to CT-like activity of purified 20S proteasome (a) incubated with DMSO or various concentrations (5, 10, 20 and 40 μM) of compound **6** for 24 h; (b) incubated with 40 μM of compound **6** for various time (0, 4, 8, 16 and 24 h) ($p < 0.001$).

Western blot assay of compound 6

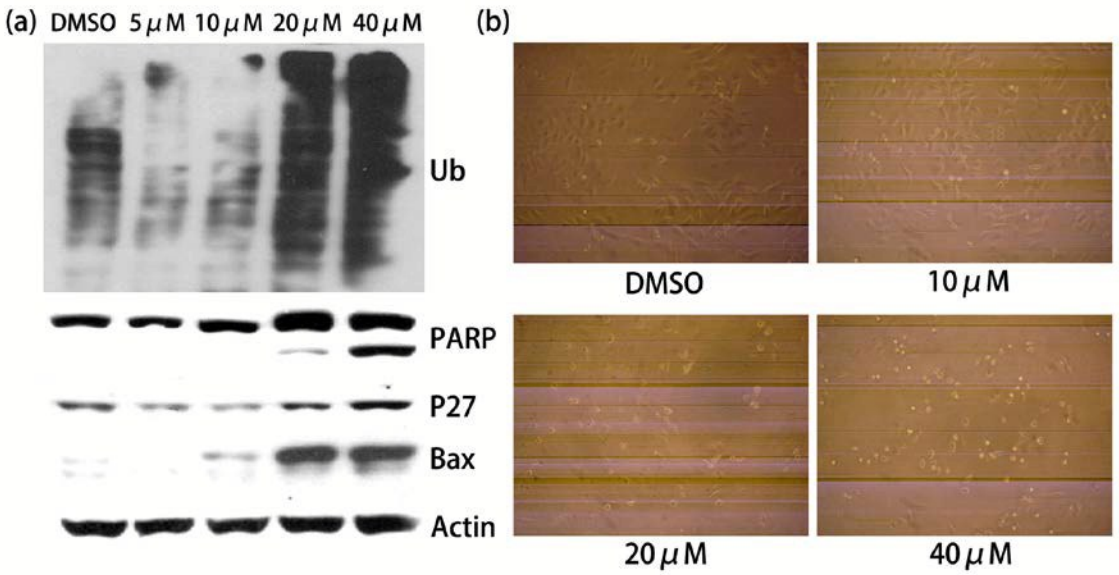

Fig 7 (a) Western blot analysis of ubiquitinated proteins, PARP, p27 and Bax, and (b) cellular morphologic changes of human liver cancer HepG2 cells (×100) treated with compound **6** at increasing concentrations (5, 10, 20 and 40 μM) for 24 h.

Human liver cancer HepG2 cells were treated with compound **6** at increasing concentrations (5, 10, 20 and 40 μM) for 24 h, followed by assessment of accumulated ubiquitinated proteins and the level of the proteasome target protein Bax and p27. Cells treated with the solvent DMSO were used as a vehicle control (Fig. 7a). The ubiquitinated proteins and the proteasome target protein Bax and p27 were accumulated in a concentration-dependent manner. In addition, the cleaved Poly (ADP-ribose) polymerase (PARP) fragment (85 kDa), a cell death-specific protein, appeared after HepG2 cells were treated with compound **6**. Consistently, morphological changes, indicative of cell death, were also observed in the same experiment (Fig. 7b). The results demonstrate that compound **6** possess proteasome inhibitory capability and cytostatic effect to human liver cancer HepG2 cells in a concentration-dependent manner

Human liver cancer HepG2 cells were treated with 40 μM of compound **6** for increasing time (0, 4, 8, 16 and 24 h), followed by Western blot analysis (Fig. 8a) and measurement of cell death (Fig. 8b). The result shows that accumulation of ubiquitinated proteins and the proteasome target protein Bax enhanced gradually as the time went on. Also, increased levels of p27 were detected at 16 and 24 h, and the cleaved p85 (PARP fragment) was observed at 24 h after HepG2 cells were treated with compound **6**. In addition, we observed morphological changes at 16 h after HepG2 cells were treated with compound **6**, and the morphological changes increased gradually with time (Fig. 8b). The results suggest that compound **6** induced proteasome inhibition and cytostatic effect to human liver cancer HepG2 cells in a time-dependent manner.

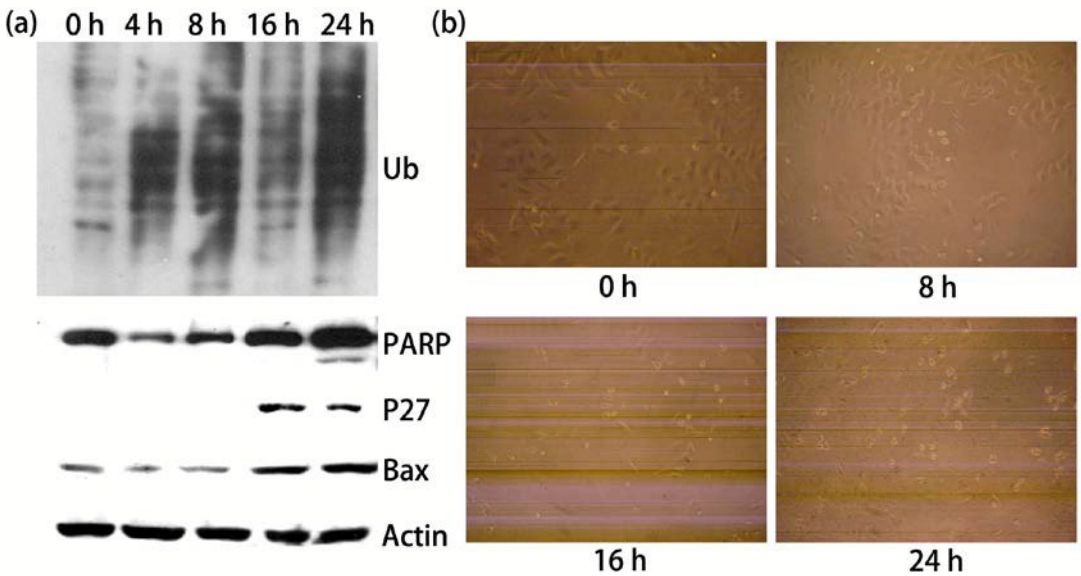

Fig 8 (a) Western blot analysis of ubiquitinated proteins, PARP, p27 and Bax, and (b) cellular morphologic changes of human liver cancer HepG2 cells (×100) treated with 40 μM of compound **6** for increasing time (0, 4, 8, 16 and 24 h).

Quantum Chemistry Calculations

Optimized geometries

The optimized molecular structures of the four tautomers of compound **6** in water environment are shown in Fig. 9. After optimization, tautomer **6d** has become tautomer **6c**, which means that tautomer **6d** cannot exist in water. Thus, only the optimized structure of tautomers **6a**, **6b** and **6c** are compared and discussed. The experimental bond lengths and torsion angles for tautomer **6c**, and the corresponding calculated values for tautomers **6a**, **6b** and **6c** are listed in Table S14 in the supplementary material. For tautomer **6c**, the optimized geometry parameters are consistent to those gained from experiments, except for some conformational discrepancies. The conformational differences is attributed to the weak intermolecular interactions between adjacent molecules in the solid state (experimental result), whereas these weak intermolecular interactions are absent in water (calculated results). Such crystal packing effects can make the phenyl rings rotate on the connecting bonds to change the conformation. The important Wiberg bond orders of tautomers **6a**, **6b** and **6c** are listed in Table 2. Fig. 9 shows the optimized molecular structure of tautomers **6a**, **6b** and **6c**.

Table 2 The important Wiberg bond orders of tautomers **6a**, **6b** and **6c**

Bond	**6a**	**6b**	**6c**
O1–C1	1.537	1.645	1.469
C1–C2	1.132	0.948	1.132
C2–C3	1.457	0.990	1.167
C2–C5	1.063	0.975	1.347
N1–C1	1.069	1.136	1.115
N1–N2	1.032	1.033	1.063
N2–C3	1.246	1.789	1.618
N3–C5	1.742	1.822	1.354

For tautomer **6a**, the bond lengths and bond orders of O1–C1, C2–C3 and N3–C5 show that they are double bonds while the bond lengths and bond orders of C1–C2, C2–C5, N1–C1, N1–N2 and N2–C3 show that they are single bonds. H2 is not coplanar with the pyrazolone ring, indicating that N2 adopts the sp3

hybridization to some extent. The steric hindrance between H2 and H24 leads to the large dihedral angle (43.7°) between the pyrazolone ring and the neighbouring phenyl ring. N3=C5 is also not coplanar with the pyrazolone ring with the large C1–C2–C5–N3 torsion angle of -37.0° and the 3.098 Å distance between O1 and N3, which is attributed to the electronic repulsion between O1 and N3. Thus, tautomer **6a** has a very low conjugation extent. The calculated total energy of tautomer **6a** is -1241.9626 a.u., and the dipole moment is 12.2875 D.

For tautomer **6b**, the bond lengths and bond orders of O1–C1, N2–C3 and N3–C5 show that they are double bonds while the bond lengths and bond orders of C1–C2, C2–C3, C2–C5, N1–C1 and N1–N2 show that they are single bonds. The dihedral angle between the pyrazolone ring and the neighbouring phenyl ring is 1.8°, indicating that the pyrazolone ring and the neighbouring phenyl ring and can form a large conjugated system. This is because H2 has transferred to connect with C2 and thereby the steric hindrance has been eliminated. Accordingly, C2 adopts the sp3 hybridization leading to the distortion of C2–C5 and increased O1···N3 seperation (3.736 Å). The total energy of tautomer **6b** is -1241.9561 a.u., and the dipole moment is 5.9126 D.

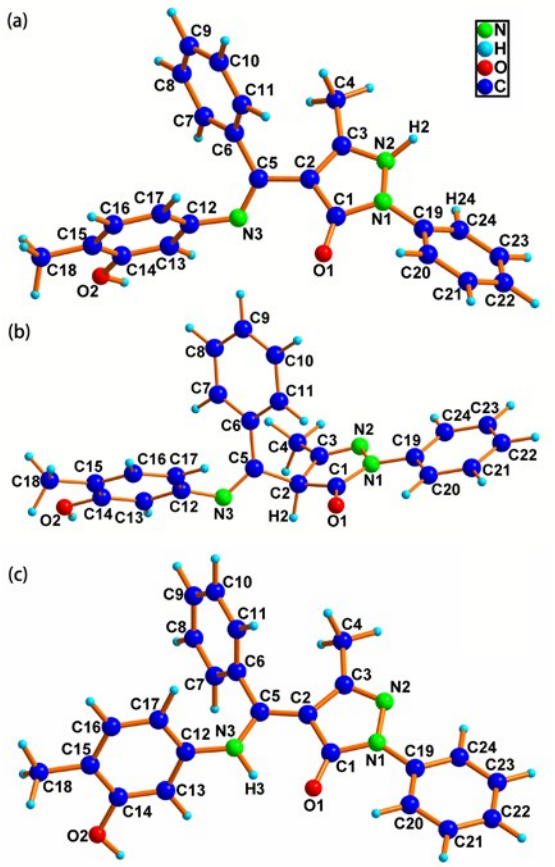

Fig. 9 The optimized molecular structure of (a) tautomer **6a**; (b) tautomer **6b**; (c) tautomer **6c**.

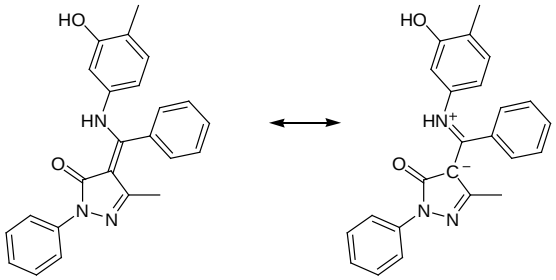

Scheme 6 Resonance between two structures of tautomer **6c**.

For tautomer **6c**, the bond lengths and bond orders of O1–C1 and N2–C3 show that they are double bonds while the bond lengths and bond orders of C1–C2, C2–C3, N1–C1 and N1–N2 show that they are single bonds. However, the bond orders of C2–C5 and N3–C5 are very similar and difficult to be assigned as double bonds or single bonds. The pyrazolone-enamine form of tautomer **6c** can actually be represented by the resonance between the two structures shown in Scheme 6, which also causes the partial separation of positive and negative charge. Considering the fact that the redundant positive charge on N3–H3 is in favor of the formation of hydrogen bonding, the partial separation of positive and negative charge might be ascribed to the formation of the intramolecular hydrogen bond N3–H3···O1. The stabilization effect of hydrogen bonding allows a closer approach between O1 and N3 (2.741 Å) and N3=C5 coplanar with the pyrazolone ring. As the dihedral angle between the pyrazolone ring and the phenyl ring is 14.4°, N3=C5, the pyrazolone ring and the neighbouring phenyl ring can form a large conjugated system. The total energy of tautomer **6c** is -1241.9839 a.u., and the dipole moment is 7.9209 D.

Since tautomer **6c** has the lowest molecular total energy and largest delocalization extent in water environment, it is the most stable and thereby the most likely existed tautomer in cancer cells. This is also consistent to the fact that tautomer **6c** is the one found in the crystal and DMSO solution. Thus, we will make the detailed discussions on tautomer **6c** to provide some information for its anticancer mechanism study.

Molecular electrostatic potential

Molecular electrostatic potential (MEP) is a useful tool to predict the sites for electrophilic and nucleophilic attacks as well as hydrogen bonding interactions, because they are associated with the electron densities in the molecule.[50] As two species can recognize each other through the potentials, the electrostatic potential V(r) are very suitable to analyze the interactions based on the recognition of two molecules like drug-receptor, and enzyme-substrate interactions.[51] To predict the possible interactive sites for tautomer **6c** with 20S proteasome through hydrogen bonding, MEP surface of tautomer **6c** was obtained based on the optimized molecular structure. The red and yellow regions in MEP are the negative regions while the blue regions represent the positive regions.

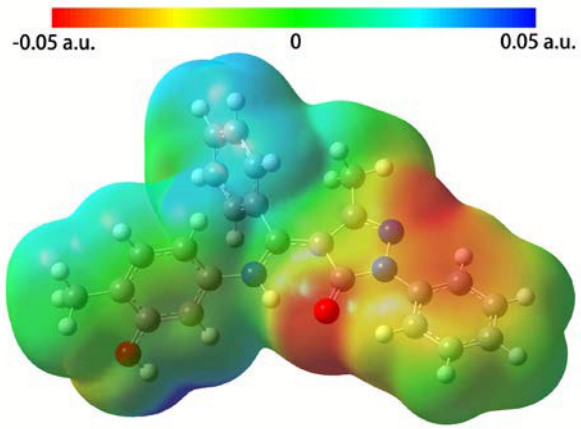

Fig. 10 The total electron density mapped with electrostatic potential surface of tautomer **6c** (for interpretation of the color, the reader is referred to the web version of this article).

As can be seen in Fig. 10, the negative regions of tautomer **6c** were found around O1 and N3 with the V(r) values of -0.058 a.u. and -0.054 a.u. Thus, it would be predicted that an electrophile would preferentially attack of tautomer **6c** at the region around O1 and N3. In contrast, the most positive region was found around the hydroxyl with the V(r) value of 0.098 a.u., indicating the possible site for nucleophilic attack. These sites can provide information concerning the regions from where tautomer **6c** can undergo hydrogen bonding interactions with 20S proteasome. Therefore, the anticancer activity of tautomer **6c** should be related to the pyrazolone ring and the hydroxyl because they are most likely engaged in hydrogen bonding as the most negative or positive regions.

Frontier molecular orbital energies and components

The frontier molecular orbitals of tautomer **6c** are shown in Fig. 11. The energies of HOMO-1, HOMO, LUMO and LUMO+1 orbitals are −0.2255, −0.2150, −0.0709, and −0.0270 a.u., respectively. Analysis of the frontier molecular orbital components shows that the frontier molecular orbital distributes nearly evenly on the molecules, which is consistent to its large extent of electron delocalization. In addition, the HOMO orbital is mainly distributed on N3=C5, the pyrazolone ring and the neighbouring phenyl ring, forming a large conjugated system. The large conjugated system makes N3=C5, the pyrazolone ring and the neighbouring phenyl ring coplanar, which could intercalate into 20S proteasome to inhibit its activity. Therefore, the anticancer activity of tautomer **6c** is also possible to be related to the plane consisted of N3=C5, the pyrazolone ring and the neighbouring phenyl ring.

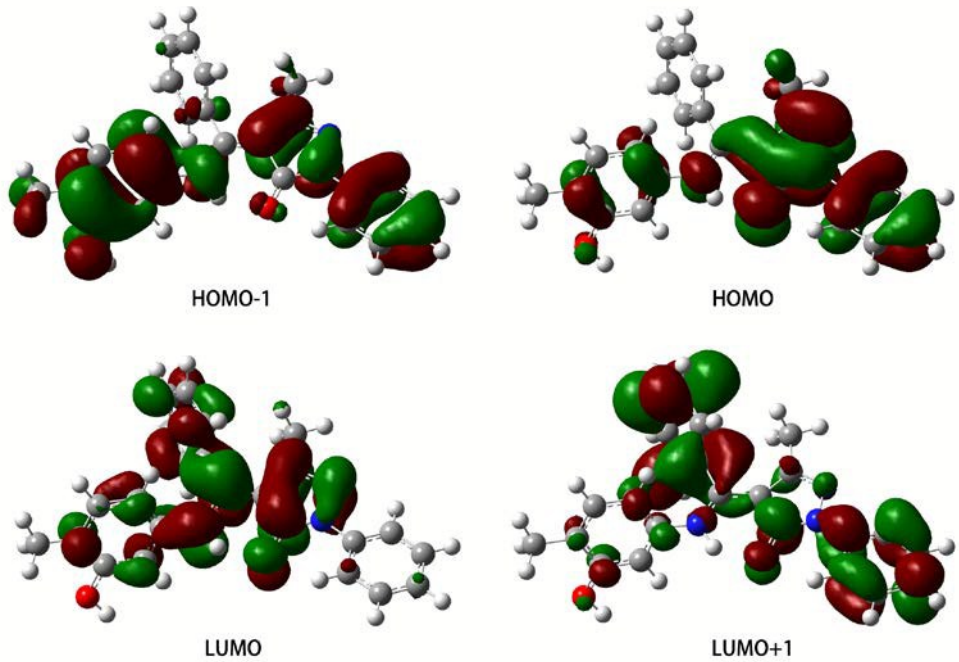

Fig. 11 View of the frontier molecular orbitals of tautomer **6c** (for interpretation of the color, the reader is referred to the web version of this article)

Conclusions

In this study the tautomerism and anticancer activities of compounds **1** ~ **9** were investigated experimentally and theoretically. Many anticancer drugs demonstrate toxicity because they are unable to distinguish the normal and tumor cells. As the cancer cells rely on proteasome more than normal cells, inhibition on the activity of proteasome could be an effective approach to resolve the problem of toxicity of anticancer drugs.[42,52,53] To study the interaction mechanism of compound **6** with 20S proteasome, we have made a detailed discussion on the tautomerism, because different tautomers may exhibit different inhibitory effect or mechanism to the activity of 20S proteasome. We have found that tautomer **6c** should be the tautomer in human cancer cells that targets 20S proteasome. It could possibly interact with 20S proteasome through hydrogen bonding formed by the pyrazolone ring and the hydroxyl, or intercalate into 20S proteasome through the plane consisted of N3=C5, the pyrazolone ring and the neighbouring phenyl ring. As a result, this kind of pyrazolone-enamine demonstrates proteasome inhibition and cytostatic effect to human cancer cells. In addition,

the position of the hydroxyl also has strong impact to the inhibitory effect. The corresponding isomers with the hydroxyl in the *meta*-position have much better anticancer activities than those in the *ortho*- or para-position. We can introduce some hydrophilic groups while retaining the pyrazolone ring and the hydroxyl in the *meta*-position to resolve the problem of low solubility in water, and design compounds with anticancer activities based on this study.

Experimental

Materials and physical measurement

All reagents used for synthesis of the nine compounds were of analytical grade and were used as obtained by commercial sources without further purification. Elemental analyses were carried out with a model 2400 Perkin-Elmer analyzer. Infrared spectra of the compounds were recorded in KBr pellets using a Nicolet 170SX spectrophotometer in the 4000 ~ 400 cm^{-1} region. ^1H NMR spectra were recorded on a Bruker DRX-600 spectrometer. The X-ray diffraction data were collected on a Bruker Smart CCD X-ray single-crystal diffractometer. The obtained single crystals were preserved in mother liquor, mounted in inert oil and transferred to the cold gas stream of the diffractometer. Other crystals were maintained at 60 °C for 24 h in an oven to remove the solvent molecules in the crystal lattice for other characterizations.

Experimental procedures of infrared spectroscopy

Take about 0.25 ~ 0.50 teaspoons of KBr and grind it with pestle in a mortar. Place just enough KBr powder to cover bottom in pellet die. Place in press and press at 5000 ~ 10000 psi. Carefully remove the pressed sample from die and place in the FT–IR sample holder to collect the background. The pressed disc should be nearly clear if properly made. Then take a little of samples on a microspatula and about 0.25 ~ 0.50 teaspoons of KBr. Mix thoroughly in a mortar while grinding with the pestle. Place just enough mixtures to cover bottom in pellet die. Place in press and press at 5000 ~ 10000 psi. Carefully remove the pressed sample from die and place in the FTIR sample holder to collect the spectra for the samples.

Experimental procedures of NMR

Weight about 10 mg samples and dissolve them in [D_6]DMSO. Then add the solvent into NMR tube. Hold the sample by the top, place sample tube in the spinner and the spinner in the sample depth gauge. Push or pull the sample tube so that the depth of the sample above and below the center line of the sample depth gauge is equal. Put NMR tube into the machine. Select experiment as proton and solvent as DMSO. Click setup hardware, stdval, auto lock and gradient shim one by one. Acquire the spectrum and make the Fourier transformation. Then save the spectrum.

Synthesis of the nine compounds

4-[(Z)-(3,5-dicarboxyphenylamino)phenylmethylene]-3-methyl-1-phenyl-2-pyrazolin-5-one (1). HPMBP (0.278 g, 1.0 mmol) dissolved in 20 mL ethanol was mixed with 5-aminoisophthalic acid (0.181 g, 1.0 mmol) dissolved in 20 mL ethanol and stirred for 4 h at 60°C. The solution obtained was filtered and the filtrate was left for slow evaporation at room temperature in the air. The yellow prismatic crystal formed after approximately 30 days. M.p. 335–340°C. Found: C, 68.11; H, 4.27; N, 9.58. Calc. for $C_{25}H_{19}N_3O_5$: C, 68.02; H, 4.34; N, 9.52%. ν_{max}/cm^{-1}: 3394, 2978, 1727, 1698, 1617, 1591, 1532, 1501, 1458, 1382, 1275, 1148, 1121, 1054, 1017, 781, 756, 727, 588. δ_H (600 MHz; [D_6]DMSO; Me_4Si) 13.34 (2H, s, COO*H*), 12.77 (1H, s; N*H*), 8.16–7.18 (15H, m, 6–*H*), 1.48 ppm (3H, s, CH_3).

4-{(Z)-[4-(4-aminobenzyl)phenylamino]phenylmethylene}-3-methyl-1-phenyl-2-pyrazolin-5-one (2). HPMBP (0.278 g, 1.0 mmol) dissolved in 20 mL methanol was mixed with 4,4′-diaminodiphenylmethane (0.198 g, 1.0 mmol) dissolved in 20 mL methanol and stirred for 4 h at 60°C. The solution obtained was filtered and the filtrate was left for slow evaporation at room temperature in the air. The brown needle crystal formed after approximately 20 days. M.p. 110–115°C. Found: C, 78.66; H, 6.80; N, 12.31. Calc. for $C_{30}H_{26}N_4O$: C, 78.58; H, 5.72; N, 12.22%. ν_{max}/cm^{-1}: 1625, 1592, 1572, 1513, 1491, 1480, 1394, 1232, 1210, 1053, 1009, 822, 777, 757, 694. δ_H (600 MHz; [D_6]DMSO; Me_4Si) 12.73 (1H, s, N*H*), 8.02–6.43 (18H, m, 6–*H*), 4.86 (2H, s, NH_2), 3.64 (2H, s, CH_2), 1.44 (3H, s, CH_3).

4-{(Z)-[4-(carboxymethyl)phenylamino]phenylmethylene}-3-methyl-1-phenyl-2-pyrazolin-5-one (3). Compound **3** was prepared using a similar procedure as that for the preparation of compound **2** but using 4-aminophenylacetic acid (0.151 g, 1 mmol) instead of 4,4′-diaminodiphenylmethane. The yellow block crystal formed after approximately 20 days. M.p. 148–151°C. Found: C, 73.44; H, 5.22; N, 10.25. Calc. for $C_{25}H_{21}N_3O_3$: C, 72.98; H, 5.14; N, 10.21%. ν_{max}/cm^{-1}: 3448, 1716, 1618, 1593, 1571, 1515, 1500, 1475, 1383, 1230, 1166, 1011, 778, 775, 690. δ_H (600 MHz; [D_6]DMSO; Me_4Si) 12.73 (1H, s, N*H*), 12.31 (1H, s, COO*H*), 8.02–6.92 (14H, m, 6–*H*), 3.60 (2H, s, CH_2), 1.45 (3H, s, CH_3).

4-{(Z)-[4-(aminocarbonyl)phenylamino]phenylmethylene}-3-methyl-1-phenyl-2-pyrazolin-5-one (4). Compound **4** was prepared using a similar procedure as that for the preparation of compound **2** but using 4-aminobenzamide (0.136 g, 1 mmol) instead of 4,4′-diaminodiphenylmethane. The yellow prismatic crystal formed after approximately 20 days. M.p. 235–240°C. Found: C, 72.68; H, 5.01; N, 14.15. Calc. for $C_{24}H_{20}N_4O_2$: C, 72.71; H, 5.08; N, 14.13%. ν_{max}/cm^{-1}: 3380, 3173, 1672, 1607, 1590, 1541, 1498, 1375, 1234, 1214, 1195, 1145, 1053, 773, 706. δ_H (600 MHz; [D_6]DMSO; Me_4Si) 12.76 (1H, s, N*H*), 8.02–7.17 (14H, m, 6–*H*), 7.00 (2*H*, d, J_{AB} 8.6, CONH_2), 1.47 (3H, s, CH_3).

4-[(Z)-(2-hydroxy-5-methylphenylamino)phenylmethylene]-3-methyl-1-phenyl-2-pyrazolin-5-one (5). Compound **5** was prepared using a similar procedure as that for the preparation of compound **2** but using 2-amino-4-methylphenol (0.123 g, 1 mmol) instead of 4,4′-diaminodiphenylmethane. The yellow block crystal formed after approximately 20 days. M.p. 284–288°C. Found: C, 75.03; H, 5.58; N, 10.88. Calc. for $C_{24}H_{21}N_3O_2$: C, 75.18; H, 5.52; N, 10.96%. ν_{max}/cm^{-1}: 3246, 1614, 1585, 1573, 1534, 1516, 1499, 1475, 1396, 1333, 1289, 1244, 1193, 1011, 841, 781, 738, 706. δ_H (600 MHz; [D_6]DMSO; Me_4Si) 12.58 (1H, s, N*H*), 10.01 (1H, s, O*H*), 8.01–6.25 (13H, m, 6–*H*), 1.88 (3H, s, PhCH_3), 1.44 (3H, s, CH_3).

4-[(Z)-(3-hydroxy-4-methylphenylamino)phenylmethylene]-3-methyl-1-phenyl-2-pyrazolin-5-one (6). Compound **6** was

prepared using a similar procedure as that for the preparation of compound **2** but using 5-amino-2-methylphenol (0.123 g, 1 mmol) instead of 4,4′-diaminodiphenylmethane. The yellow block crystal formed after approximately 20 days. M.p. 203–206°C. Found: C, 75.22; H, 5.47; N, 11.02. Calc. for $C_{24}H_{21}N_3O_2$: C, 75.18; H, 5.52; N, 10.96%. ν_{max}/cm^{-1}: 3207, 1611, 1589, 1526, 1499, 1479, 1446, 1386, 1294, 1238, 1185, 1053, 997, 848, 756, 687. δ_H (600 MHz; [D_6]DMSO; Me_4Si) 12.67 (1H, s, N*H*), 9.52 (1H, s, O*H*), 8.01–6.24 (13H, m, 6–*H*), 2.00 (3H, s, PhCH_3), 1.44 (3H, s, CH_3).

4-[(Z)-(2-hydroxyphenylamino)phenylmethylene]-3-methyl-1-phenyl-2-pyrazolin-5-one (7). Compound **7** was prepared by the method in the literature.[54,55] HPMBP (4.170 g, 15.0 mmol) dissolved in 30 mL ethanol was mixed with 2-aminophenol (1.635 g, 15.0 mmol) dissolved in 20 mL ethanol and stirred for 4 h at 80°C give a yellow precipitate. The precipitate was filtered off and recrystallized from ethanol. M.p. 298–302°C. Found: C, 74.71; H, 5.24; N, 11.45. Calc. for $C_{23}H_{19}N_3O_2$: C, 74.78; H, 5.18; N, 11.37%. ν_{max}/cm^{-1}: 1618, 1581, 1501, 1464, 1397, 1332, 1283, 1224, 1181, 1148, 1094, 1067, 1010, 747, 694, 650, 583, 497. δ_H (600 MHz; [D_6]DMSO; Me_4Si) 12.60 (1H, s, N*H*), 10.27 (1H, s, O*H*), 8.01–6.49 (14H, m, 6–*H*), 1.43 (3H, s, CH_3).

4-[(Z)-(3-hydroxyphenylamino)phenylmethylene]-3-methyl-1-phenyl-2-pyrazolin-5-one (8). Compound **8** was prepared using a similar procedure as that for the preparation of compound **7** but using 3-aminophenol (1.635 g, 15.0 mmol) instead of 2-aminophenol. M.p. 236–238°C. Found: C, 74.88; H, 5.13; N, 11.36. Calc. for $C_{24}H_{21}N_3O_2$: C, 74.78; H, 5.18; N, 11.37%. ν_{max}/cm^{-1}: 3446, 3062, 1587, 1490, 1387, 1174, 1055, 1005, 846, 764, 696. δ_H (600 MHz; [D_6]DMSO; Me_4Si) 12.69 (1H, s, N*H*), 9.61 (1H, s, O*H*), 8.01–6.35 (14H, m, 6–*H*), 1.44 (3H, s, CH_3).

4-[(Z)-(4-hydroxyphenylamino)phenylmethylene]-3-methyl-1-phenyl-2-pyrazolin-5-one (9). Compound **9** was prepared using a similar procedure as that for the preparation of compound **7** but using 4-aminophenol (1.635 g, 15.0 mmol) instead of 2-aminophenol. M.p. 267–270°C. Found: C, 74.84; H, 5.13; N, 11.39. Calc. for $C_{24}H_{21}N_3O_2$: C, 74.78; H, 5.18; N, 11.37%. ν_{max}/cm^{-1}: 3419, 3250, 1614, 1507, 1470, 1392, 1261, 1221, 1145, 839, 760, 697, 648, 607, 545, 507. δ_H (600 MHz; [D_6]DMSO; Me_4Si) 12.60 (1H, s, N*H*), 9.56 (1H, s, O*H*), 8.02–6.57 (14H, m, 6–*H*), 1.43 (3H, s, CH_3).

Crystallographic data collection and structure determination

Diffraction intensity data of the single crystals of compounds **1** ~ **6** were collected on a Bruker Smart CCD X-ray single-crystal diffractometer equipped with a graphite monochromated MoKα radiation (λ = 0.71073 Å) by using a φ and ω scan mode at 298(2) K. The programs used for data collection and cell refinement are the SMART and SAINT programs.[56] Empirical absorption correction was applied using the SADABS programs,[57] The structures refinements were against F^2 by the full-matrix least-squares technique using the SHELXTL crystallographic software package,[58] All non-hydrogen atoms were found in the final difference Fourier map. The hydrogen atoms involved in tautomeric reactions were also found from difference Fourier maps and refined without constraints. The methyl H atoms were positioned geometrically and refined using a riding model, with C–H = 0.96 Å and $U_{iso}(H) = 1.5\ U_{eq}(C)$. All the other hydrogen atoms were fixed geometrically at calculated distances and allowed to ride on the parent non-hydrogen atoms. Positional and thermal parameters were refined by full-matrix least-squares method to convergence. The crystallographic data of compounds **1** ~ **6** are summarized in Table S1.

Anticancer activity studies

Biological reagents and antibodies

Stock solutions of compounds were prepared by dissolution in DMSO (20 mM) and stored at −20 °C. DMEM/F-12, RPMI-1640, penicillin, and streptomycinwere purchased from Invitrogen (Carlsbad, CA). Fetal bovine serum was purchased from Tissue Culture Biologicals (Tulare, CA). Purified 20S proteasome (rabbit) was purchased from Boston Biochem. Fluorogenic peptide substrate Suc-LLVY-AMC was purchased from Calbiochem (San Diego, CA). Rabbit monoclonal antibody against human poly (ADP-ribose) polymerase (PARP) and Bax (B-9) was purchased from Biomol International LP (Plymouth Meeting, PA). Mouse monoclonal antibodies against Ub and p27, and goat polyclonal antibody against actin (C-11) and all secondary antibodies were purchased from Santa Cruz Biotechnology Inc. (Santa Cruz, CA). The concentrations of all antibodies were 200 μg/mL.

Cell cultures and whole-cell extract preparation

HepG2 human liver cancer cells were obtained from American Type Culture Collection (Manassas, VA) and grown in DMEM/F-12 media supplemented with10% fetal bovine serum, 100 U/mL penicillin, and 100 μg/mL streptomycin. The media were supplemented with 10% fetal calf serum, 100 U/mL of penicillin, and 100 mg/mL of streptomycin. All cells were maintained at 37˚C and 5% CO_2. A whole-cell extract was prepared as previously described.[59–61]

Proteasomal CT-like activity in cell extracts

Whole-cell extracts (4 μg) were incubated for 2 h at 37˚C in 100 μL assay buffer (50 mM Tris-HCl, pH 7.5) with 20 μM fluorogenic substrate Suc-LLVY-AMC specific for the CT-like activity. After incubation, production of hydrolyzed AMC groups was measured with a Wallac Victor 3 Multilabel Counter with an excitation filter of 365 nm and emission filter of 460 nm. Changes in fluorescence were calculated against the DMSO treated control.

Inhibition of purified 20S proteasome activity

Briefly, 0.1 mg of purified 20S rabbit proteasome was incubated with 20 mM fluorogenic substrate Suc-LLVY-AMC specific for the CT-like activity for 30 min at 378 in 100 mL of assay buffer (50 mM Tris–HCl (pH = 7.5)) with different concentrations of samples. After incubation, production of hydrolyzed AMC groups were measured using a multi-well plate VersaFluorTM Fluorometer with a Wallac Victor 3 Multilabel Counter with an excitation filter of 365 nm and an emission filter of 460 nm.

Cellular morphologic analysis

A Zeiss Axiovert-25 microscope was used for all microscopic imaging with phase contrast for cellular morphology, and cells that become shrunken and rounded up were considered as dead cells.

Western blot analysis

Equal amounts of cell lysate (40 μg) were resolved by SDS-polyacrylamide gel electrophoresis, transferred to a nitrocellulose membrane and blotted with indicated antibodies followed by visualization with the enhanced chemiluminescence reagent

(Amersham Biosciences, Piscataway, NJ).

Computational details

Optimizations of geometrical structures and Natural Bond Orbital (NBO) analyses of compounds **6** were carried out by DFT B3LYP method with 6-31+G* basis set combined with PCM in water. The harmonic vibrational frequencies were calculated at the same level of theory for the optimized structure. The vibrational frequency calculations revealed no imaginary frequencies, indicating that a stationary point at this level of approximation was found for the compounds. Atom coordinates used in the calculations were based on the four tautomers of HPMBP optimized by F. Caruso *et. al.*[62] All calculations were conducted on a Pentium IV computer using Gaussian 03 program.[63] To investigate the reactive sites of tautomer **6c** the molecular electrostatic potential was evaluated. The molecular electrostatic potential, V(**r**), at a given point **r**(x, y, z) in the vicinity of a molecule, is defined in terms of the interaction energy between the electrical charge generated by the molecule's electrons and nuclei and a positive test charge (a proton) located at **r**.

Acknowledgements

This research was supported by the Specialized Research Fund for the Doctoral Program of Higher Education of China (grant No. 20120132110015), the National Natural Science Foundation of China (grant Nos. 21371161, 21071134 and 20971115), the Special Foundation for Young Teachers of Ocean University of China (grant No. 201113025) and the Natural Science Foundation of Shandong Province (grant No. ZR2012BQ026)

Notes and references

[a] *Key Laboratory of Marine Chemistry Theory and Technology, Ministry of Education, College of Chemistry and Chemical Engineering, Ocean University of China, Qingdao , Shandong 266100, P. R. China. Tel: 86 0532 66781932; E-mail: fanyuhua301@163.com (Y. Fan), bicaifeng301@163.com (C. Bi)*

[b] *Qingdao Institute of Bioenergy and Bioprocess Technology, Chinese Academy of Sciences, Qingdao, 266101, P. R. China*

[c] *Key Laboratory of Sustainable Development of Marine Fisheries, Ministry of Agriculture, Yellow Sea Fisheries Research Institute, Chinese Academy of Fishery Sciences, Qingdao, 266071, P. R. China*

† Electronic Supplementary Information (ESI) available: characterization of the position of the hydrogen atom, crystallographic data and structure refinement for compounds **1** ~ **6**, selected bond lengths and angles for compounds **1** ~ **6**, the hydrogen bonding geometry for compounds **1** ~ **6** and the optimized geometry parameters for tautomers **6a**, **6b** and **6c**. CCDC 949389 (**1**), 889325 (**2**), 881279 (**3**), 886801 (**4**), 887652 (**5**) and 912501 (**6**). For ESI and crystallographic data in CIF or other electronic format, see DOI: 10.1039/b000000x/

1 M. A. Ali, M. Shaharyar and A. A Siddiqui, *Eur. J. Med. Chem.*, 2007, **42**, 268−275.
2 J. Matysiak and A. Niewiadomy, *Bioorg. Med. Chem.*, 2003, **11**, 2285−2291.
3 M. E. Shoman, M. Abdel-Aziz, O. M. Aly, H. H. Farag and M. A. Morsy, *Eur. J. Med. Chem.*, 2009, **44**, 3068−3076.
4 Z. H. Chohan, M. H. Youssoufi, A. Jarrahpour and T. Ben Hadda, *Eur. J. Med. Chem.*, 2010, **45**, 1189−1199.
5 N. Mishra and D. Sasmal, *Bioorg. Med. Chem.*, 2011, **21**, 1969−1973.
6 N. D. Amnerkar and K. P. Bhusari, *Eur. J. Med. Chem.*, 2010, **45**, 149−159.
7 P. C. Ly, D. D. Li, Q. S. Li, X. Lu, Z. P. Xiao and H. L. Zhu, *Bioorg. Med. Chem.*, 2011, **21**, 5374−5377.
8 M. A. Ali, M. S. Yar, A. A Siddiqui, D. Sriram, P. Yogeeswari and E. De Clercq, *Acta Pol. Pharm.*, 2007, **64**, 328−423.
9 J. L. Wang, Y. Yang, X. Zhang and F. M. Miao, *Acta Cryst.*, 2003, E**59**, o430−o432.
10 S. Umetani, K. Sasayama and M. Matsui, *Anal. Chim. Acta*, 1982, **134**, 327–331.
11 Y. Akama, A. Tong, S. Ishima and M. Kajitani, *Anal. Sci*., 1992, **106**, 250–253.
12 Y. Akama, T. Nakai and F. Kawamura, *Analyst*, 1981, **106**, 250–253.
13 Y. Akama, T. Nakai and F. Kawamura, *Bunseki Kagaku*, 1976, **25**, 496–500.
14 B. A. Omotow and M. A. Mesubi, *Appl. Organomet. Chem.*, 1997, **11**, 1–10.
15 E. C. Okafor, *Spectrochim. Acta A*, 1981, **37**, 945–950.
16 K. P. Balasubramanian, K. Parameswari, V. Chinnusamy, R. Prabhakaran and K. Natarajan, *Spectrochim. Acta A*, 2006, **65**, 678–683.
17 R. Campo, J. J. Criado, E. Garcia, M. R. Hermosa, A. J. Sanchez, J. L. Manzano, E. Monte, E. R. Fernandez and F. Sanz, *J. Inorg. Biochem.*, 2002, **89**, 74–82.
18 R. Karvembu, S. Hemalatha, R. Prabhakaran, K. Natarajan, *Inorg. Chem. Commun.*, 2003, **6**, 486–490.
19 T. D. Thangadurai and K. Natarajan, *Trans. Met. Chem.*, 2002, **27**, 485–489.
20 G. D. Frey, Z. R. Bell, J. C. Jeffery and M. D. Ward, *Polyhedron*, 2001, **20**, 3231–3237.
21 F. Mevellec, S. Collet, D. Deniand, A. Reliquet and J. C. Meslin, *J. Chem. Soc., Perkin Trans.*, 2001, **1**, 3128–3131.
22 M. M. Omar, G. G. Mohamed and A. M. M. Hindy, J. Therm, *Anal. Calorim.*, 2006, **86**, 315–325.
23 J. Z. Wu and L. Yuan, *J. Inorg. Biochem.*, 2004, **98**, 41–45.
24 Z. H. A. El-Wahab, M. M. Mashaly, A. A. Salman, B. A. El-Shetary and A. A. Faheim, *Spectrochim. Acta A*, 2004, **60**, 2861–2873.
25 M. A. Baseer, V. D. Jasdhav, R. M. Phule, Y. V. Archana and Y. B. Vibhute, *Orient. J. Chem.*, 2000, **16**, 553–556.
26 S. K. Sridhar, S. N. Pandeya and E. De Clercq, *Boll. Chim. Farm.*, 2001, **140**, 302–305.
27 W. M. Singh, B. C. Dash, *Pesticides*, 1998, **22**, 33–37.
28 G. F. Liu, T. S. Shi and Y. N. Zhao, *J. Mol. Struct.*, 1997, **412**, 75–81.
29 B. P. Das, R. T. Choudhury, K. G. Das, D. N. Choudhury and B. Choudhury, *Chem. Environ. Res.*, 1994, **3**, 19–23.
30 F. Sparatore, G. Pirisino, M. C. Alamanni, P. Maca-Dimich and M. Satta, *Boll. Chim. Farm.*, 1978, **117**, 638–651.
31 H. Shiff, *Ann. Chem. Pharm. Suppl.*, 1864, **3**, 343–370.
32 A. T. Chaviara, P. C. Christidis, A. Papageorgiou, E. Chrysogelou, D. J. Hadjipavlou-Litina and C. A. Bolos, *J. Inorg. Biochem.*, 2005, **99**, 2102–2109.
33 J. L. Wang, S. M. Zhang, X. Zhang and F. M. Miao, *Huaxue Xuebao*, 2003, **61**, 1071-1076.
34 J. Zuo, C. F. Bi, Y. H. Fan, D. Buac, C. Nardon, K. G. Daniel and Q. P. Dou, *J. Inorg. Biochem.*, 2013, **118**, 83-93
35 R. Z. Orlowski and E. C. Dees, *Breast Cancer Res.*, 2003, **5**, 1–7.
36 K. R. Landis-Piwowar, V. Milacic, D. Chen, H. Yang, Y. Zhao, T. H. Chan, B. Yan and Q. P. Dou, *Drug Resist. Updat.*, 2006, **9**, 263–273.
37 S. V. Rajkumar, P. G. Richardson, T. Hideshima and K. C. Anderson, *J. Clin. Oncol.*, 2005, **23**, 630–639.
38 Z. Zhang, C. F. Bi, D. Buac, Y. H. Fan, X. Zhang, J. Zuo, P. F. Zhang, N. Zhang, L. L. Dong and Q. P. Dou, *J. Inorg. Biochem.*, 2013, **123**, 1–10.
39 A. Clechanover, *Cell*, 1994, **79**, 13–21.
40 B. An, R. H. Goldfarb, R. Siman and Q. P. Dou, *Cell Death Differ.*, 1998, **5**, 1062–1075.
41 U. G. Lopes, P. Erhardt, R. Yao and G. M. Cooper, *J. Biol. Chem.*, 1997, **272**, 12893–12896.
42 Q. P. Dou and B. Li, *Drug Resist. Updat.*, 1999, **2**, 215–223.
43 Z. Zhang, C. F. Bi, S. M. Schmitt, Y. H. Fan, L. L. Dong, J. Zuo and Q. P. Dou, *J. Biol. Inorg. Chem.*, 2012, **17**, 1257–1267.
44 E. Seemuller, A. Lupas, D. Stock, J. Lowe, R. Huber and W. Baumeister, *Science*, 1995, **268**, 579–582.
45 H. J. Yang, D. Chen, Q. C. Cui, X. Yuan and Q. P. Dou, *Cancer Res.* 2006, **66**, 4758–4765.

46 A. Anaflous, N. Benchat, M. Mimouni, S. Abouricha, T. Ben-Hadda, B. El-Bali, A. Hakkou and B. Hacht, *Lett. Drug. Des. Discov.*, 2004, **1**, 224–229.

47 Z. H. Chohan, S. H. Sumrra, M. H. Youssoufi and T. Ben-Hadda, *Eur. J. Med. Chem.*, 2010, **45**, 2739–2747.

48 B. Bennani, A. Kerbal, M. Daoudi, B. Filali-Baba, G. Al-Houari, A. F. Jalbout, M. Mimouni, M. Benazza, G. Demailly, M. Akkurt, S. Öztürk Yıldırım and T. Ben-Hadda, *Arkivoc*, 2007, **xvi**, 19–40.

49 L. da Costa Souza, R Camargo, M Demasi, J. M. Santana, C. M. de Sá and S. M. de Freitas, *PLoS One*, 2014, **9**, e86600.

50 N. Okulik and A. H. Jubert, *Internet Electron. J. Mol. Des.*, 2005, **4**, 17–30.

51 P. Politzer, P. R. Laurence, K. Jayasuriya and J. McKinney, *Environ. Health Perspect.*, 1985, **61**, 191–202.

52 J. Adams, *Drug Discov. Today*, 2003, **8**, 307–315.

53 J. B. Almond and G. M. Cohen, *Leukemia*, 2002, **16**, 433–443.

54 J. L. Wang, S. M. Zhang, X. Zhang and F. M. Miao, *Huaxue Xuebao*, 2003, **61**, 1071-1076..

55 K. Saida, B. Fatiha, D. Ouarda, O. Ali, O. Kamel and L. Brelot, *Acta Cryst.*, 2012, E**68**, o1909-o1910.

56 SMART and SAINT, Area Detector Control and Integration Software, Siemens Analytical X-ray Systems, Inc., Madison, WI, 1996.

57 Bruker AXS, SAINT Software Reference Manual, Madison, WI, 1998.

58 G. M. Sheldrick, *Acta Cryst.*, 2008, A**64**, 112–122.

59 Y. Akama, T. Nakai and F. Kawamura, *Bunseki Kagaku*, 1976, **25**, 496–500.

60 K. P. Balasubramanian, K. Parameswari, V. Chinnusamy, R. Prabhakaran and K. Natarajan, *Spectrochim. Acta A*, 2006, **65**, 678–683.

61 X. Zhang, C. F. Bi, Y. H. Fan, C. Cui, D. Chen and Q. P. Dou., *Int. J. Mol. Med.*, 2008, **22**, 677-682.

62 F. Caruso, C. Pettinari, F. Marchetti, M. Rossi, C. Opazo, S. Kumar, S. Balwani and B. Ghosh, *Bioorg. Med. Chem.*, 2009, **17**, 6166–6172.

63 K. D. Frisch, G. W. Trucks, H. B. Schlegel, M. A. Robb, J. R. Cheeseman, V. G. Zakrzewski and J. A. Montgomery, Gaussian03, (Revision A.6), Gaussian, Inc., Pittsburgh, PA, 2003.